MAPPING PADDY FIELD IN EAST JAPAN USING SENTINEL-1 TIME SERIES ASSISTED BY SENTINEL-2

Shimpei Inoue (1), Chinatsu Yonezawa (2), Akihiko Ito (1)

[1] National Institute for Environmental Studies, 2 16 Onogawa, Tsukuba, Ibaraki, Japan
[2] Tohoku University, 1 468 Aoba, Aramaki, Aoba-ku, Sendai, Miyagi, Japan
Email: inoue.shinpei@nies.go.jp ; chinatsu.yonezawa.e7@tohoku.ac.jp ; itoh@nies.go.jp

KEY WORDS: paddy field mapping, remote sensing, Sentinel-1, Sentinel-2

ABSTRACT: The distribution of paddy fields affects greatly regional budget of methane (CH_4), which is the second influential greenhouse gas. Therefore, broad scale paddy field map is fundamentally important for methane budget estimation. However, only a few paddy field maps have been developed, because there remain serious technical issues making it difficult. For example, rice cultivation period overlaps roughly with rainy and cloudy seasons and differs among regions due to complicated factors such as rice cultivar and water management. To solve these problems, several methods using Sentinel-1 time series have been proposed, because it is robust against cloud-cover conditions. However, these methods that use only Sentinel-1 time series have an issue in accuracy of extracting paddy field, because the SAR sensor of Sentinel-1 is less sensitive to vegetation and flooded condition than optical sensors with multi-bands. In this study, to compensate for the weakness of Sentinel-1 time series in paddy field mapping, we propose a new method assisted by Sentinel-2, which is more reliable and robust for the extraction of flooded condition over various land surfaces. Our new method consists of two major steps. In Step 1, paddy fields were provisionally extracted by the thresholds based on the seasonal variation and the flooded condition using the time series of VH-polarized backscatter of Sentinel-1A. In Step 2, among the pixels specified to be provisional paddy field in Step 1, those which were classified as 'non-flooded' by the LSWI, NDVI and EVI calculated using the Sentinel-2 data during a flooded period, were excluded. Finally, we developed a paddy field map for East Japan in 2018 with 30m spatial resolution. The results show that our proposed method assisted by Sentinel-2 was effective in reducing mis-classifications especially for areas cultivated by other crops.

1. INTRODUCTION

Paddy fields play important roles in various environmental issues including food security, water resource management, biodiversity conservation and climate change. Especially in terms of climate change, paddy field is one of the major sources of methane (CH_4), which is the second influential greenhouse gas for global warming following CO_2. The distribution of paddy fields affects greatly regional methane budget. In Japan, the methane emission from paddy fields occupies more than 40% of the total methane budget (Ito, 2019). Therefore, broad scale paddy field maps are fundamentally important for improving the accuracy of methane budget estimations. With increasing necessity of paddy field maps at national to global scales, many efforts have been made by using satellite remote sensing images including optical images and synthetic aperture radar (SAR) images. Before the 2010s, the most of studies for broad scale paddy field mapping used limited types of remote sensing images with relatively low to middle spatial resolution, such as MODIS (Takeuchi, 2004, Xiao, 2005 and Ozdogan, 2008). Processing multisource remote sensing images at high spatial and temporal resolutions on a broad scale is a major challenge, because it needs large computer storage and high operating capacity (Zhang, 2018). Recent years, remote sensing analyses on cloud-based platforms such as Google Earth Engine (GEE) have become popular, making it possible to easily use huge amount of multisource remote sensing images with higher spatial resolution. However, only a few paddy field maps have been developed, because there remain serious technical issues making it difficult. For example, rice cultivation period overlaps roughly with rainy and cloudy seasons and differs among regions due to complicated factors such as rice cultivar and water management. To solve these issues, several methods using Sentinel-1 time series have been proposed, because it is robust against cloud-cover conditions. However, these methods that use only Sentinel-1 images have an issue in accuracy of extracting paddy field, because the backscatter of Sentinel-1 is less sensitive to vegetation and flooded condition than optical sensors with multi-bands (Torbick, 2017). In this study, to compensate for the weakness of Sentinel-1 time series in paddy field mapping, we propose a new method to reduce mis-classification in mappings assisted by Sentinel-2, which is more reliable and robust for the extraction of flooded condition over various land surfaces. We developed a paddy field maps for East Japan in 2018 with 30m spatial resolution. Compared with the paddy field maps developed by our method and those by the conventional method using only Sentinl-1 time series, the potential of our method for broad scale paddy field mapping are demonstrated.

2. STUDY AREA & DATA

2.1 Study Area

Eastern part of Japan, including Hokkaido prefecture, Tohoku area, Kanto area and Niigata prefecture (24.2 – 45.7N, 137.6 – 145.9E), was selected as a study area (Figure 1). The area includes several important rice production bases of Japan. According to the statistics announced by Ministry of Agriculture, Forestry and Fisheries of Japan (MAFF), the total paddy field area with rice planting in 2018 was approximately 9,016 km² and occupied about 4.6 % of the total area of the study area 195,389 km². Approximately 4.5 million tons of rice was produced in 2018, which accounted for about 60% of total rice production of Japan.

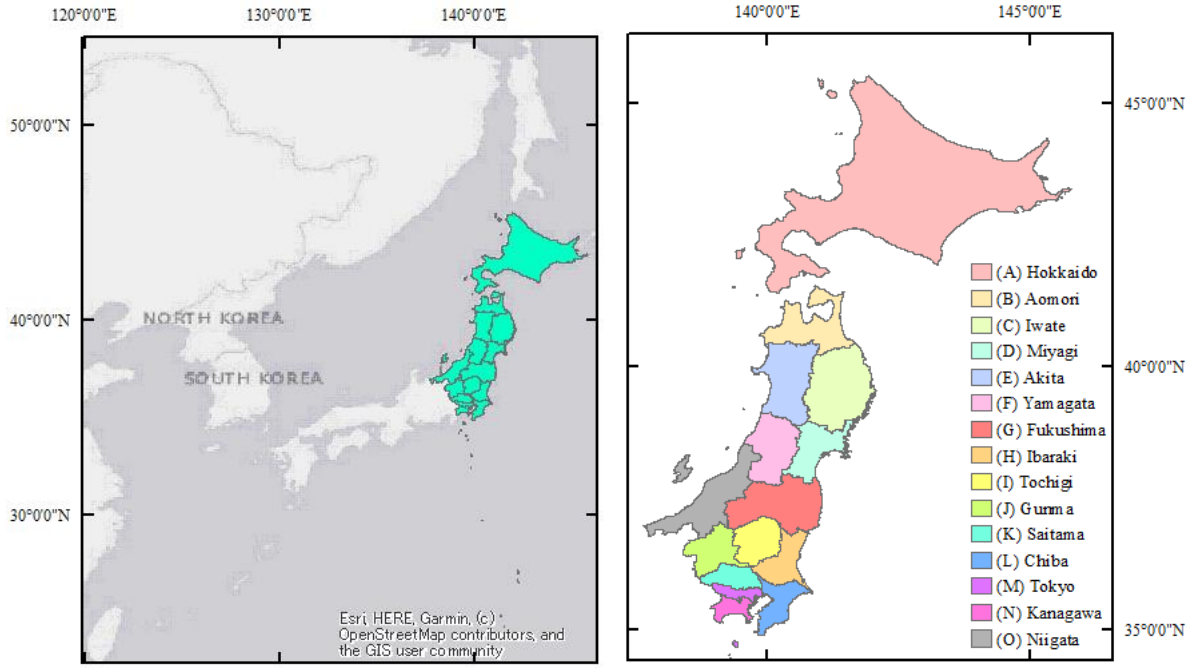

Figure 1: Location map of the study area including 15 prefectures. In this paper, these 15 prefectures are indicated by the capital letter "(A)" to "(O)".

2.2 Sentinel-1A time series

Sentinel-1 satellites were launched by the European Space Agency (ESA) on 3 April 2014 (Sentinel-1A) and 25 April 2016 (Sentinel-1B). The SAR sensor aboard the satellite acquires images at C-band with 5.4 GHz in 4 modes, namely Strip map (SM), Interferometric Wide Swath (IW), Extra Wide (EW) and Wave, with different spatial resolutions and swath widths. We used images acquired in IW mode, which acquires images with a swath width of 250 km and 5 m × 20 m spatial resolution. To minimize the effects of orbit directions and look angles, we only used images that acquired by Sentinel-1A satellite from a descending orbit with VH polarization. In this study, we focused on VH polarization, because previous studies show that VH-polarized backscatter is more sensitive to rice phenology than other polarizations (Nguyen, 2016 and Mansaray, 2017). Sentinel-1A satellite has a 12-days revisit cycle at the equator. Therefore, most of the study area are observed more than 30 times per year. From GEE, we accessed the Sentinel-1A time series, which consist of the all Sentinel-1A Ground Range Detected (GRD) images acquired from the "Transplant Start date" to the "Harvest End date" announced by MAFF in Table 1.

2.3 Sentinel-2 MSI images

Sentinel-2 satellites were launched by the ESA on 23 June 2015 (Sentinel-2A) and 7 March 2017 (Sentinel-2B). Both satellites have a 10-days revisit cycle respectively. And the satellites carry Sentinel-2 Multispectral Instrument (MSI), which is an optical sensor with 12 bands acquiring images with a swath width of 290km and 10-60 m spatial resolution. From GEE, we accessed the Sentinel-2 MSI Level-1C Top of Atmosphere (TOA) reflectance images acquired from the "Transplant Start date" to the "Harvest End date" in the study area by both satellites.

Table 1: Cultivation dates of each prefecture, which are average dates from 2015 to 2017 announced by MAFF. (A) to (O) correspond to those in Figure 1.

	(A)	(B)	(C)	(D)	(E)	(F)	(G)	(H)
Transplant Start	19-May	15-May	10-May	3-May	15-May	13-May	9-May	28-Apr
Transplant End	30-May	27-May	25-May	21-May	29-May	25-May	26-May	25-May
Harvest End	10-Oct	16-Oct	20-Oct	15-Oct	15-Oct	14-Oct	23-Oct	29-Sep

	(I)	(J)	(K)	(L)	(M)	(N)	(O)
Transplant Start	1-May	22-May	28-Apr	18-Apr	29-May	18-May	4-May
Transplant End	14-Jun	26-Jun	27-Jun	10-May	28-Jun	12-Jun	20-May
Harvest End	17-Oct	1-Nov	26-Oct	17-Sep	20-Oct	21-Oct	3-Oct

2.4 Reference data

Two classes of reference fields, “Paddy field” and “Not paddy field”, were prepared for accuracy assessments. Using Google map Street View, 100 paddy fields were selected as “Paddy field” from each of the 6 prefectures, (A)Hokkaido prefecture, (B)Aomori prefecture, (F)Yamagata prefecture, (H)Ibaraki prefecture, (N)Kanagawa prefecture and (O)Niigata prefecture (Figure 2a). These 6 prefectures were selected because in some parts of these prefectures the Street Views were taken during the flooded period of paddy fields in 2018. By visual interpretations, the fields that were flooded and planted rice were selected as “Paddy fields”. Flooding management during cultivated period is a distinctive feature of rice different from other major crops. On the other hand, the agricultural field polygons released from MAFF were used as “Not paddy fields”. The agricultural field polygons were derived from high spatial resolution aerial photos. And the agricultural field polygons are specified “Paddy field” or “Not paddy field” by visual interpretations. To remove the uncertainty of the visual interpretations, 8 cities were selected where rice was not planted at all in 2018 based on national statistics released from MAFF (Figure 2b and 2c). The all agricultural field polygons specified “Not paddy field” of the 8 cities consisted reference fields of “Not paddy field”. The reference data consisted of 600 fields for “Paddy field” and 43,269 fields for “Not paddy field”.

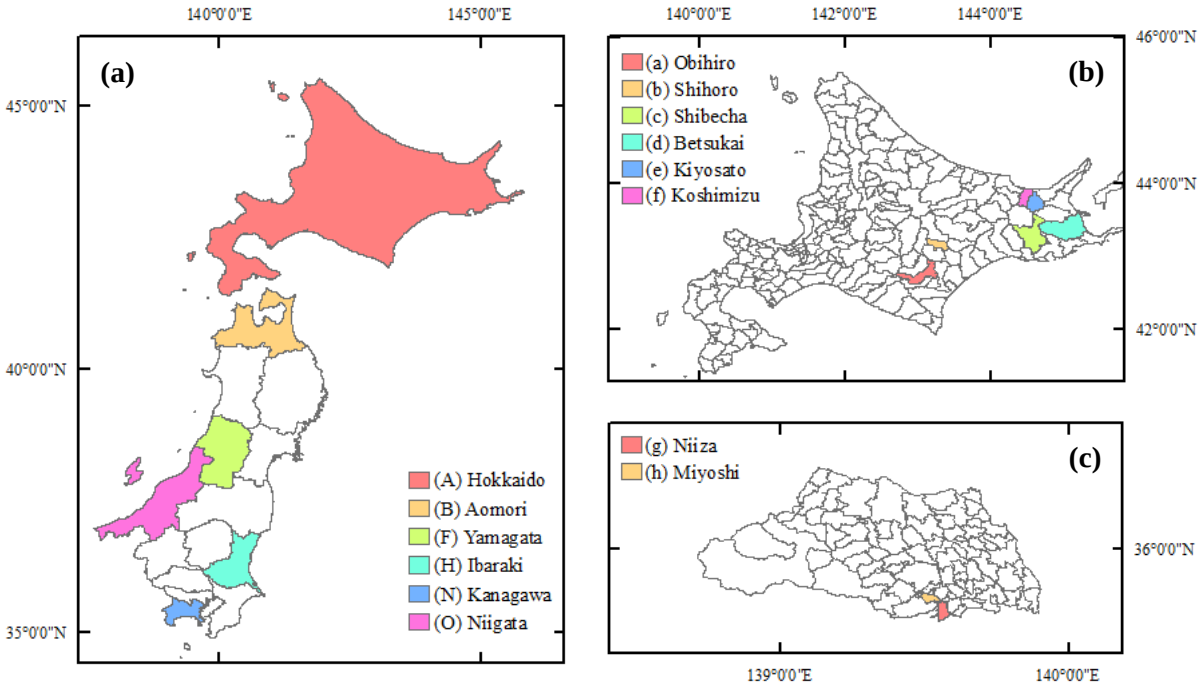

Figure 2: (a) 6 prefectures from which reference fields of “Paddy field” were selected. All agricultural fields of (b) 6 cities in Hokkaido prefecture (A in Figure 1) and 2 cities in Saitama prefecture (K in Figure 1) were used as reference fields of “Not paddy field”.

3. METHOD & VALIDATION

A comprehensive flow chart is shown in Figure 3. In this study, two types of paddy field maps were developed by “S-1 method” and “S-1 & S-2 method” at each of the 15 prefectures in the study area. The all processes in the flow chart except accuracy assessment were performed in GEE.

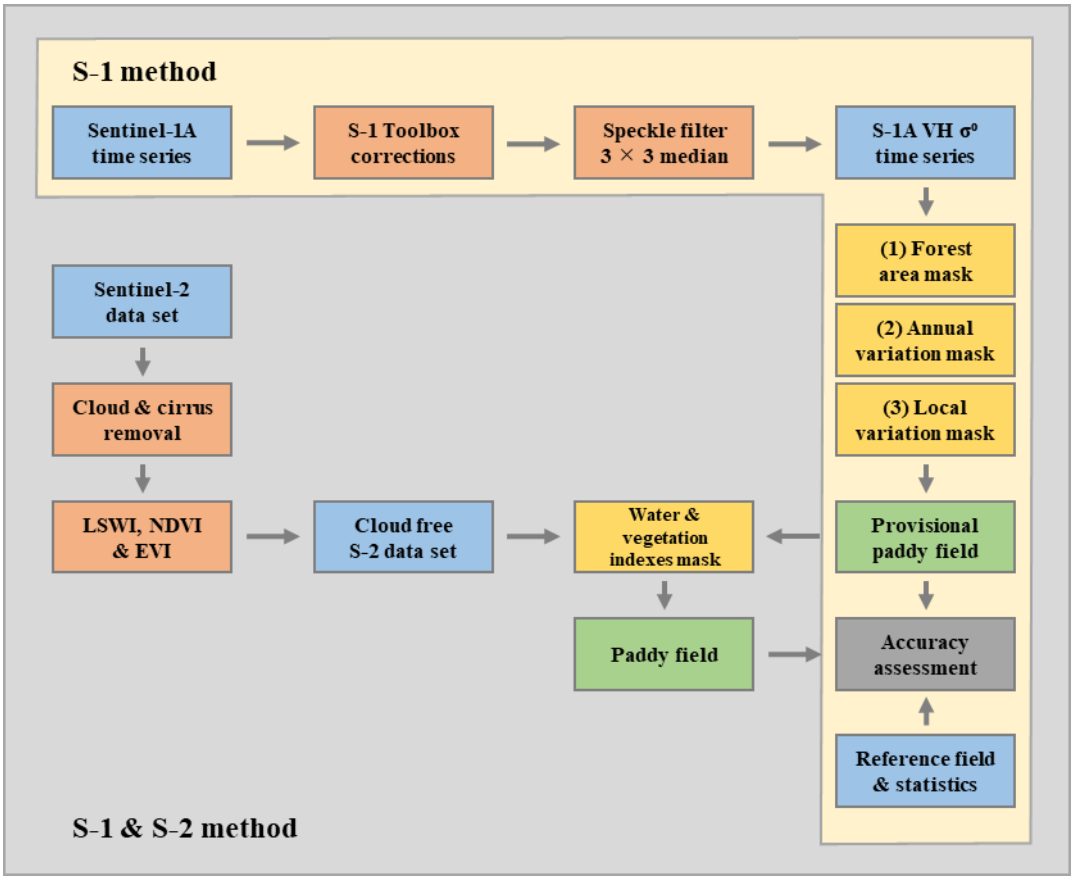

Figure 3: Flow chart of the paddy field mapping by "S-1 method" and "S-1 & S-2 method"

3.1 Preprocessing

The Sentinel-1A images that we accessed from GEE platform have been preprocessed using the Sentinel-1 Toolbox developed by the ESA to generate the backscatter coefficient σ^0 with 5 steps, (1) Apply orbit file, (2) ground range detected border noise removal, (3) thermal noise removal, (4) radiometric calibration, (5) terrain correction. For these preprocessed images, we applied the median filter with 3 × 3 pixels moving window to reduce inherent speckle noise of SAR data (Mandal, 2018).
Sentinel-2 MSI images are greatly influenced by cloud conditions. Therefore, the pixels including clouds and cirruses were removed from all Sentinel-2 MSI images according to Quality Assessment (QA60) band. Finally, cloud-free Sentinel-2 MSI datasets were readied.

3.2 Step 1; Extracting provisional paddy field using Sentinel-1A time series "S-1 method"

In Step 1, paddy field areas were provisionally extracted by the decision tree method using 3 masks described below for the time series of VH-polarized backscatter of Sentinel-1A. Decision tree methods using Sentinel-1 time series based on characteristics of rice phenology are one of the conventional methods for paddy field mapping (Nguyen, 2016, Mansaray, 2017, Clauss, 2018 and Bazzi, 2019).
(1) Forest area mask; A mask for forest area was made based on Hansen Global Forest Change v1.6 (2000-2018) which have been updated from the original Hansen's map (Hansen, 2013). The pixels including a forest area more than 30% of a pixel area were specified as a forest pixel. In the Hansen's map, forest area is defined by canopy closure for all vegetation taller than 5m in height.
(2) Annual variation mask; The annual maximum σ^0 value and the annual minimum σ^0 value of the Sentinel-1A time series were calculated each pixel. And, the pixels that have the annual maximum σ^0 smaller than −17 dB or annual minimum σ^0 larger than −20dB, were masked. These conditions are valid to differentiate vegetation with clear seasonality, such as crops and deciduous forests, from land cover with a constantly low backscatter, such as waterbodies, or high backscatter, such as urban areas (Clauss, 2018).
(3) Local variation mask; The local maximum σ^0 value and the local minimum σ^0 value of Sentinel-1A time series within 90 days moving windows were calculated for each Sentinel-1A image consisting the Sentinel-1A time series. The temporal σ^0 signal of paddy fields has very distinct minima when the paddy fields are flooded and maxima at the heading stage of the rice plants (Clauss, 2018). The pixels that the local minimum σ^0 larger than −22 dB or the

local maximum smaller than −17 dB, were masked for each Sentinel-1A images.
The Forest area masking was performed to minimize commission error for mapping paddy field (Dong, 2016). And, the Annual variation masking was performed to reduce the amount of calculation for Local variation masking. It should be noted that the Forest area masking and the Annual variation masking were performed for the entire Sentine-1A time series, whereas the Local variation masking was performed for each Sentinel-1A image consisting Sentinel-1A time series. The pixels of Sentinel-1A images during a flooded term that were not masked by above 3 types of masking, were extracted as a provisional paddy field. The flooded period means the period from the "Transplant Start date" to the date calculated by adding 30 days to "Transplant End date" in this study. We call the series of processes in Step 1 "S-1 method" in this paper. A paddy field map was developed by "S-1 method" for the purpose of comparison with a paddy field map developed by our proposed method.

3.3 Step 2; Reclassifying provisional paddy field assisted by Sentinel-2 "S-1 & S-2 method"

In Step 2, the provisional paddy field was reclassified based on water and vegetation indexes calculated from Sentienl-2 MSI images during the flooded period. Three optical-band indexes, Land Surface Water Index (LSWI), Normalized Difference Vegetation Index (NDVI) and Enhanced Vegetation Index (EVI) were calculated in each Sentinel-2 MSI image during the flooded period. The LSWI is known to be sensitive to the total amount of liquid water in vegetation and its soil background (Chandrasekar, 2010). And, the NDVI and the EVI are known to be sensitive to the variations of vegetations. These three indexes were calculated using the following equations:

$$\mathrm{LSWI} = \frac{\mathrm{NIR} - \mathrm{SWIR}}{\mathrm{NIR} + \mathrm{SWIR}} \tag{1}$$

$$\mathrm{NDVI} = \frac{\mathrm{NIR} - \mathrm{Red}}{\mathrm{NIR} + \mathrm{Red}} \tag{2}$$

$$\mathrm{EVI} = \frac{2.5 \times (\mathrm{NIR} - \mathrm{Red})}{\mathrm{NIR} + 6 \times \mathrm{Red} - 7.5 \times \mathrm{Blue} + 1} \tag{3}$$

where Blue, Red, NIR and SWIR are the top of atmosphere reflectance values of the B2 band (Central wavelength: 492 nm), B4 band (665 nm), B8 band (832 nm) and B11 band (1610-1614nm) in the Sentinel-2 MSI. Previous studies have revealed that relationship between LSWI, NDVI, and EVI can effectively extract flooded condition (Gao, 1996 and Boschetti, 2014). For each Sentinel-1A image to which the 3 masking were applied in Step 1, a local maximum "LSWI – NDVI" and "LSWI – EVI" value within 10 days after the date that the Sentinel-1A image acquired were calculated. The pixels that the local maximum "LSWI – NDVI" and "LSWI – EVI" are both smaller than -0.1 were masked. The pixels of Sentinel-1A images during a flooded term that were not masked by above 4 types of masking in Step 1 and Step 2, were extracted as a paddy field finally. We call the series of processes in both Step 1 and Step 2 "S-1 & S-2 method" in this paper.

3.4 Accuracy assessment

The accuracies of paddy field maps were assessed by producer's accuracies based on pixel-scale. The producer's accuracy indicates the quality of the classifications and be calculated by dividing the correctly classified pixels in each category by the number of reference set pixels of the corresponding category. All pixels of paddy field maps spatially included in two types of reference fields polygons were subjects to accuracy assessments. The processes of accuracy assessments were performed in ArcMap 10.5.1.

4. RESULT & DISCUSSION

4.1 Result

The producer's accuracies of "Paddy field" and "Not paddy field" are shown in table 2. The producer's accuracies were 58.7-86.3% by "S-1 method" and 82.7-85.0% by "S-1 & S-2 method". Furthermore, the producer's accuracies of each "Paddy field" and "Not paddy field" reference regions are shown in table 3 and table 4, respectively. The producer's accuracies of each of the "Paddy field" reference regions were 76.8-100.0% by "S-1 method" and 76.3 – 100.0% by "S-1 & S-2 method". The producer's accuracies of each of the "Not paddy field" reference regions were 52.7-99.5% by "S-1 method" and 74.0 – 99.6% by "S-1 & S-2 method". The paddy field maps developed by "S-1 method" and "S-1 & S-2 method" are shown in Figure 4, and total paddy field areas of the two paddy field maps and official announced values by MAFF are shown in Table 5.

Table 2: Accuracy assessment for paddy field mapping.

Method	Accuracy type	Paddy field	Not paddy field
S-1 method	Producer's accuracy	86.3%	58.7%
S-1 & S-2 method	Producer's accuracy	85.0%	82.7%

Table 3: Producer's accuracies of each "Paddy field" reference region.

Method	(A)	(B)	(F)	(H)	(N)	(O)
S-1 method	91.0%	83.2%	81.9%	76.8%	81.1%	100.0%
S-1& S-2 method	88.4%	83.2%	80.0%	76.3%	80.3%	100.0%

Table 4: Producer's accuracies of each "Not paddy field" reference region.

Method	(a)	(b)	(c)	(d)	(e)	(f)	(g)	(h)
S-1 method	69.9%	52.7%	55.7%	56.9%	66.8%	55.7%	99.5%	94.4%
S-1& S-2 method	97.2%	97.8%	74.3%	74.0%	95.3%	93.6%	99.6%	95.7%

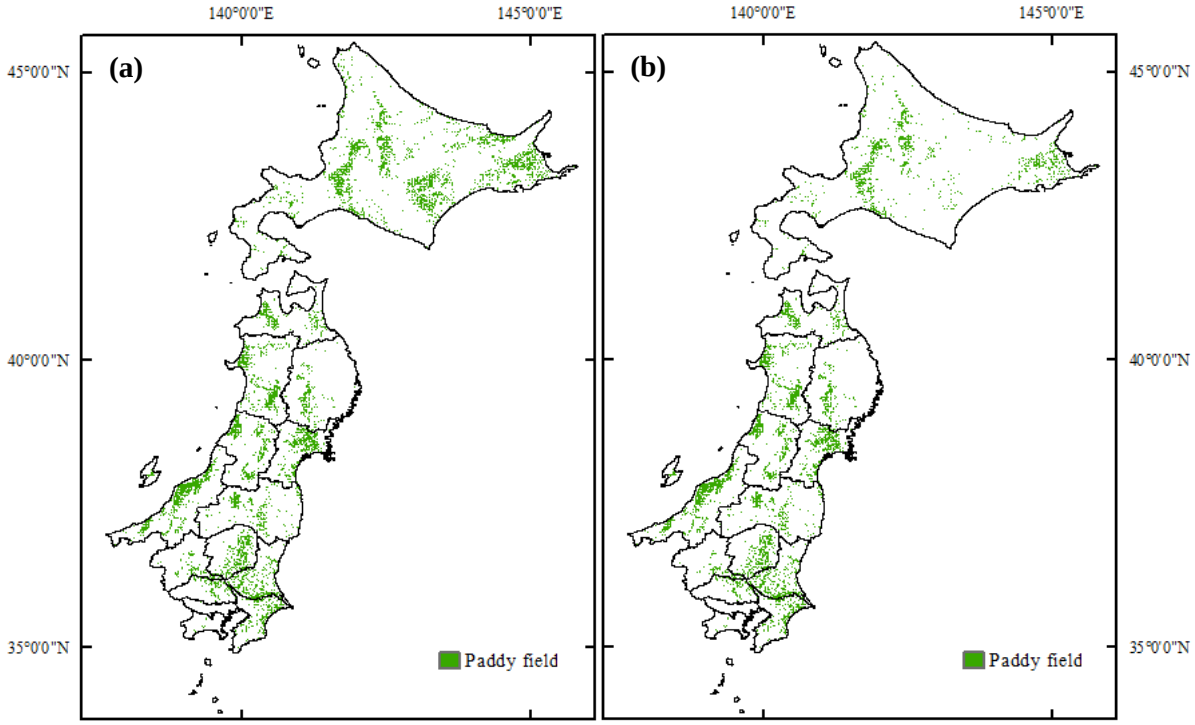

Figure 4: Paddy field maps developed by (a) "S-1 method" and (b) "S-1 & S-2 method"

Table 5: Total paddy field areas of the two maps developed by "S-1 method" and "S-1 & S-2 method", and official announced values from MAFF. (A) to (O) correspond to those in Figure 1.

	(A)	(B)	(C)	(D)	(E)	(F)	(G)	(H)
S-1 method (ha)	492,812	55,129	44,255	79,126	93,527	70,688	60,552	68,363
S-1 & S-2 method (ha)	252,464	52,663	42,094	73,977	90,708	64,905	56,107	66,066
MAFF (ha)	106,400	50,300	55,900	74,900	90,900	69,100	71,200	77,000

	(I)	(J)	(K)	(L)	(M)	(N)	(O)	Total
S-1 method (ha)	55,468	18,197	27,531	51,646	312	1,740	132,872	**1,252,218**
S-1 & S-2 method (ha)	52,783	13,946	26,039	50,444	255	1,661	126,333	**970,445**
MAFF (ha)	69,300	17,300	33,600	61,000	133	3,090	121,500	**901,623**

4.2 Discussion

This study shows the potential of our proposed paddy field mapping method "S-1 & S-2 method", which uses Sentinel-1A time series assisted by Sentinel-2, by comparing with a conventional paddy field mapping method "S-1 method", which uses only Sentienl-1A time series. The results of the producer's accuracies in Table 2 show that the "S-1 & S-2 method" was 1.3 point lower than the "S-1 method" for "Paddy field", but 24.0 point higher for "Not paddy field". The "S-1 & S-2 method" performed one more masking than "S-1 method" for extracting of paddy field, therefore the producer's accuracy of "Paddy field" by "S-1 & S-2 method" was necessarily lower than it by "S-1 method". However, the difference between the two producer's accuracies of paddy field was only 1.3 point, and so we believe it does not seriously affect the accuracy of paddy field extraction. Therefore, the "S-1 & S-2 method" is considered to be one of effective paddy field mapping approaches by reducing mis-classification in "Not paddy field".

However, the results in Table 4 shows that the effects for reducing mis-mapping by the "S-1 & S-2 method" were different among the regions. The first possible cause of the inter-regional variation in accuracy is gaps of the Sentinel-2 data due to clouds covering. Because there aren't any cloud-free Sentinel-2 images during the flooded period, the masking in Step 2 could be ineffective. Other causes that could make the differences of the effects are differences of cultivated crops, but the true cause has not been clarified in this study.

As confirmed in Table 3, the producer's accuracies of the paddy field by the two methods were different among the reference regions. The maximum difference was 23.7 point between Ibaraki prefecture and Niigata Prefecture by "S-1 & S-2 method". The local minimum threshold that intends for extracting flooded conditions, in the Local variation mask are set referring to the existing studies (Clauss, 2018, Mandal, 2018 and Bazzi, 2019) that intends for mapping paddy fields outside Japan. However, flooding management methods greatly differ among regions according to climate, water resource, cultivar and other factors. Therefore, even in the study area, the best threshold should be selected depending on the regions.

The results in Table 5 shows that the paddy maps developed in this study, overestimated in Hokkaido prefecture. Compared with other prefectures, the field area that cultivated crops other than rice in Hokkaido prefecture is much larger. Furthermore, most of fields are leveled very flat before planting crops. In this case the Sentinel-1A time series might show the similar time series variations to the paddy field. Therefore, it is considered that many mis-classifications in "Not paddy field", which could not be removed even with the mask in Step 2, remained.

5. CONCLUSION

This study demonstrated the potential of our new paddy field mapping method using Sentinel-1A time series assisted by Sentinel-2 to compare to the conventional paddy field method using only Sentinel-1A time series.

Our method including the additional mask based on the LSWI, NDVI and EVI calculated from the Sentinel-2 MSI images during the flooded period, was more effective than the conventional method without Sentinel-2 for reducing mis-classification in cultivated fields other than paddy fields.

However, the effects for reducing mis-classification were different depending on the regions. These differences were possibly attributable to complicated factors such as the gaps of Sentinel-2 cloud-free images and the differences of cultivated crops.

Although our method showed the great effect for reducing mis-classifications, the producer's accuracy of "Paddy field" reference fields was not satisfactory values, and mis-classifications remain especially in Hokkaido prefecture. In order to further improve accuracies of broad scale paddy field mapping, it is necessary to make great efforts such as finding the optimal threshold value that is more appropriate for the characteristics of paddy fields in the region.

Reference

Bazzi, H. et al., 2019, Mapping paddy rice using Sentinel-1 SAR time series in Camargue, France. In *Remote sensing, 11, 7, 887.*

Boschetti, M. et al., 2014, Comparative analysis of Normalised Difference Spectral Indices derived from MODIS for detecting surface water in flooded rice cropping systems. In *PLOS, 10, 1371, 88741.*

Chandrasekar, K. et al., 2010, Land Surface Water Index (LSWI) response to rainfall and NDVI using the MODIS Vegetation Index product. In *International Journal of Remote Sensing, 31, 15, 3987-4005.*

Clauss, K. et al., 2018, Mapping rice areas with Sentinel-1 time series and superpixel segmentation. In *International Journal of Remote sensing, 39, 5, 1399-1420.*

Dong, J. et al., 2016, Mapping paddy rice planting area in northeastern Asia with Landsat 8 images, phenology-based algorithm and Google Earth Engine. In *Remote Sensing of Environment, 185, 142-154.*

Gao, B., 1996, NDWI—A normalized difference water index for remote sensing of vegetation liquid water from space. In *Remote Sensing of Environment, 580, 3, 257-266.*

Hansen, M, C. et al.., 2013, High-Resolution Global Maps of 21st-Century Forest Cover Change. In *Science, 342, 6160, 850-853.*

Ito, A. et al., 2019, Methane budget of East Asia, 1990–2015: A bottom-up evaluation. In *Science of The Total Environment, 676, 40-52.*

Mandal, D. et al., 2018, A processing chain for differentiating early and late transplanted rice using time-series Sentinel-1 SAR data with Google Earth Engine. In *IEEE Geoscience and Remote Sensing Letters, 15, 12, 1947-1951.*

Mansaray, L. et al., 2017, Mapping rice fields in urban Shanghai, southeast China, using Sentinel-1A and Landsat8 datasets. In *Remote Sens, 9, 257.*

Nguyen, B, D. et al., 2016, Mapping rice extent and cropping scheme in the Mekong Delta using Sentinel-1A data. *In Remote Sensing Letters, 7, 12, 1209-1218.*

Ozdogan, M. et al., 2008, A new methodology to map irrigated areas using multi-temporal MODIS and ancillary data: An application example in the continental US. *In Remote Sensing of Environment, 112, 9, 3520-3537.*

Takeuchi, W. et al., 2004, Mapping of fractional coverage of paddy fields over East Asia using MODIS data. In *Journal of the Japan society of photogrammetry and remote sensing, 43, 6, 20-33.*

Tian, H. et al., 2018, Mapping early, middle and late rice extent using Sentinel-1A and Landsat-8 data in the Poyang Lake Plain, China. In *Sensors, 18, 185.*

Torbick, N. et al., 2017, Monitoring rice agriculture across Myanmar using time series Sentinel-1 Assisted by Landsat-8 and PALSAR-2. In *Remote sensing, 9, 2, 119.*

Xian, X. et al., 2005, Mapping paddy rice agriculture in southern China using multi-temporal MODIS images. In *Remote Sensing of Environment, 95, 4, 480-492.*

Zhang, X. et al., 2018, Mapping up-to-date paddy rice extent at 10m resolution in China through the integration of optical and synthetic aperture radar images. In *Remote Sensing, 10, 8, 1200.*